

# *s*-process enrichment and the origin of barium in ultrafaint dwarf galaxies

Yuta Tarumi<sup>1\*</sup>, Takuma Suda<sup>2,3,4</sup>, Robert J. J. Grand<sup>5</sup>, Freeke van de Voort<sup>5,6</sup>, Shigeki Inoue<sup>7,8</sup>, Naoki Yoshida<sup>1,3,9</sup>

<sup>1</sup>*Department of Physics, School of Science, The University of Tokyo, Bunkyo, Tokyo 113-0033, Japan*

<sup>2</sup>*Department of Liberal Arts, Tokyo University of Technology, Ota-ku, Tokyo 144-8535, Japan*

<sup>3</sup>*Research Center for the Early Universe, School of Science, The University of Tokyo, Bunkyo-ku, Tokyo 113-0033, Japan*

<sup>4</sup>*Open University of Japan, Mihama-ku, Chiba 261-8586, Japan*

<sup>5</sup>*Max Planck Institute for Astrophysics, Karl-Schwarzschild-Strasse 1, 85748, Garching, Germany*

<sup>6</sup>*School of Physics and Astronomy, Cardiff University, Queens Buildings, The Parade, Cardiff CF24 3AA, UK*

<sup>7</sup>*Center for Computational Sciences, University of Tsukuba, Ten-nodai, 1-1-1 Tsukuba, Ibaraki 305-8577, Japan*

<sup>8</sup>*Chile Observatory, National Astronomical Observatory of Japan, Mitaka, Tokyo 181-8588, Japan*

<sup>9</sup>*Kavli Institute for the Physics and Mathematics of the Universe (WPI), UTIAS, The University of Tokyo, Chiba 277-8583, Japan*

Accepted XXX. Received YYY; in original form ZZZ

## ABSTRACT

Recent spectroscopic observations of ultrafaint dwarf galaxies (UFDs) revealed that the small, old galaxies contain a substantial amount of neutron-capture elements such as Barium (Ba), Strontium (Sr) and Europium (Eu). We use cosmological simulations to study the production of Ba in UFDs. Ba is produced by both *r*- and *s*-processes, and one can infer the contribution of the *r*-process from the characteristic *r*-process abundance pattern, whereas the *s*-process contribution remains largely unknown. We show that the current *s*-process yield from asymptotic giant branch (AGB) stars is not sufficient to explain the Ba abundances observed in UFDs. Ba production would need to be efficient from the beginning of star formation in the galaxies. The discrepancy of nearly 1 dex is not reconciled even if we consider *s*-process in super-AGB stars. We consider a possible resolution by assuming additional Ba production with short delay time. Considering the diversity of Ba abundances among different UFDs, a rare and prolific source is favoured. Fast-rotating massive stars could be such rare and prolific sources, and they can account for the observed abundance if  $\sim 3 \times 10^{-10} M_{\odot}$  of Ba is produced per  $1 M_{\odot}$  formed stars. We also explore another resolution by modifying the stellar initial mass function (IMF) in UFDs, and find a particular IMF model that reproduces the observed level of Ba-enrichment. We argue that future observations that determine or tightly constrain the Eu abundance are crucial to identify the origin of Ba in UFDs.

**Key words:** galaxies:dwarf – stars: abundances – stars: AGB and post-AGB – galaxies: abundances – methods: numerical

## 1 INTRODUCTION

Neutron-capture processes are important for the synthesis of the heaviest elements. They are classified into two processes: *r*-process and *s*-process, by whether neutron-capture reactions occur faster than  $\beta$ -decays (see, e.g. Cowan et al. 2019). Neutron-rich environments are necessary for neutron-capture reactions to take place, but the origin or the astrophysical production site remains controversial for the *r*-process (Cowan et al. 2019; Nishimura et al. 2017). On the contrary, it is generally thought that the *s*-process occurs mainly in low mass stars during their asymptotic giant branch (AGB) phase.

Two major neutron-capture elements, Barium (Ba) and Strontium (Sr), are relatively easy to detect in stellar spectra. For solar metallicity stars, these elements are largely synthesized by the *s*-process. However, since the main contributors of the *s*-process are low-mass and long-lived stars, they contribute to the Galactic chemical evolution only slowly. This feature is consistent with the observations of Milky-Way (MW) stars which show monotonic increase of [Ba/Fe] as

the iron (Fe) abundance [Fe/H] increases. At low Fe abundances, as typically found in ultrafaint dwarf galaxies (UFDs), we cannot consider Ba to be produced entirely by the *s*-process. In fact, theoretical studies find that both Ba and Sr are also produced by the *r*-process in MW and dwarf galaxies (Cescutti et al. 2006; Hirai et al. 2019). UFDs have several distinct features in terms of their chemical evolution, which make them particularly interesting objects (Simon 2019). One important feature is the predominantly old stellar population. It is theoretically expected that the shallow gravitational potential well is inefficient at retaining gas after cosmic reionization (Brown et al. 2014). Another important trait that makes UFDs particularly interesting objects is the stochasticity of *r*-process enrichment. For UFDs, rare enrichment events imprint particularly strong signatures. For example, a typical *r*-process element, europium (Eu), is detected only in three UFDs out of  $\sim 15$  UFDs. A natural interpretation of the diversity of Eu abundances among the UFDs is that *r*-process events are rare and prolific (Ji et al. 2016a; Hansen et al. 2020). Typically, UFDs are chemically less evolved systems, and thus provide important insight into the early chemical evolution in the Universe. Recently detailed chemical abundances of metal-poor stars in UFDs

\* E-mail: yuta.tarumi@phys.s.u-tokyo.ac.jp

have been obtained (e.g. [Frebel et al. 2014](#); [Ishigaki et al. 2014](#); [Chiti et al. 2018](#); [Ji et al. 2019a](#)). These observations consistently suggest that, for those without clear *r*-process signatures, there is a deficit of neutron-capture elements (including Ba and Sr) in UFD compared to Milky-Way stars. In the present paper we model the *s*-process enrichment of UFDs. We use cosmological simulations to follow the star formation and chemical enrichment, which are outlined in Section 2. The characteristic star formation histories and the small stellar masses of UFDs provide clues to understand the chemical enrichment history of neutron-capture elements. We show the simulation results in Section 3. In Section 4, we argue that the existence of an additional Ba source is strongly suggested to explain the observed elemental abundances in UFD stars.

## 2 METHOD

### 2.1 Cosmological Simulations

We use `AREPO`, a moving-mesh hydrodynamic simulation code ([Springel 2010](#); [Pakmor et al. 2016](#); [Weinberger et al. 2019](#)). As the cosmological parameters, we use the Planck 2018 results ([Planck Collaboration et al. 2018](#)):  $\Omega_m = 0.315$ ,  $\Omega_b = 0.049$ ,  $\sigma_8 = 0.810$ ,  $n_s = 0.965$ ,  $H_0 = 67.4 \text{ km s}^{-1} \text{ Mpc}^{-1}$ . The code settings and galaxy formation models are the same models as in the Auriga simulations ([Grand et al. 2017](#)). The initial conditions are generated using `MUSIC` ([Hahn & Abel 2011](#)). The boxsize is 1 comoving  $h^{-1} \text{ Mpc}$  on a side. We use a hierarchical zoom-in technique to resolve the inner structure of the small simulated galaxies. The mass of each dark-matter particle is about  $100 M_\odot$ , and the typical mass of each gas cell and star particle is about  $20 M_\odot$ . From our previous paper we select two galaxies ‘halo 1’ and ‘halo 3’ as the galaxy samples ([Tarumi et al. 2020](#)). In this paper, we refer to halo 1 as the ‘large UFD’ and halo 3 as the ‘small UFD’. In Fig. 1 we present the star formation histories of our galaxy samples. Halo mass ( $M_h$ ), stellar mass ( $M_*$ ), and size ( $R_{200}$ ) of these samples are  $(M_h, M_*, R_{200}) = (1.7 \times 10^8 M_\odot, 2.0 \times 10^4 M_\odot, 1.717 \text{ kpc})$ , and  $(8.7 \times 10^7 M_\odot, 3,000 M_\odot, 1.544 \text{ kpc})$ , respectively at redshift  $z = 8$ , which can be regarded as UFD progenitors ([Safarzadeh et al. 2018](#)). These haloes grow to  $(M_h, M_*, R_{200}) = (2.7 \times 10^8 M_\odot, 2.0 \times 10^4 M_\odot, 3.917 \text{ kpc})$ , and  $(3.1 \times 10^8 M_\odot, 2,600 M_\odot, 4.061 \text{ kpc})$  by redshift  $z = 4$  which is our final snapshot. Basic properties such as the growth of stellar and gas masses are insensitive to the change of the resolution (see [Tarumi et al. 2020](#)).

### 2.2 Chemical evolution

In our hydrodynamics simulations, the gas density field and stars are represented by gas cells and star particles, respectively. The gas cells contain elemental abundance information. Each star particle represents a cluster of stars. It enriches the surrounding gas cells with metals. The amounts of elements distributed to nearby cells in one time-step are determined as follows. First, we specify the mass range of stars that contribute to chemical enrichment within the next time-step by age and metallicity of the star particle. Next, we integrate the elemental yields from the stars that die within the time-step assuming the Chabrier’s initial mass function (IMF) ([Chabrier 2001](#)). We use the *s*-process yield table from `FRUITY` database ([Cristallo et al. 2015, 2016](#)) for low-metallicity stars and ([Karakas & Lugaro 2016](#)) for high-metallicity stars. Finally, we distribute the calculated amounts of elements to nearby gas cells in the smoothed-

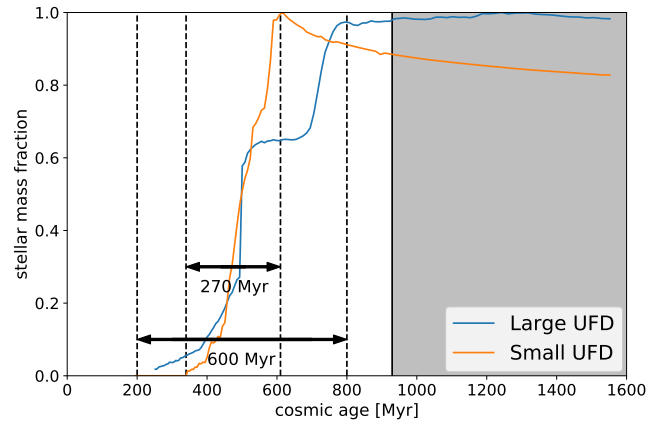


**Figure 1.** Star formation histories of our simulated galaxies. Blue curve: ‘large UFD’, which forms stars for  $\sim 600$  Myr. The peak stellar mass is  $\sim 20,000 M_\odot$ . Orange curve: ‘small UFD’, which forms stars for  $\sim 300$  Myr. The peak stellar mass is  $\sim 3,500 M_\odot$ . The ‘large UFD’ experienced a major merger at a cosmic age of  $\sim 500$  Myr at redshift 10. The shaded area shows when the Universe is ionized and no or little star formation is expected in UFDs.

particle-hydrodynamics manner. The procedure is performed for each star particle at each time-step.

We note that the masses of star particles in our high-resolution simulations are too small to sample massive stars with sufficient frequency. Such insufficient sampling could result in artificial elemental distributions in the galaxy. However, the synthesis of *s*-process elements occurs only in AGB stars, whose progenitors are  $3\text{--}8 M_\odot$  stars in our simulations. The expected number of stars between 3 to  $8 M_\odot$  is 0.6 for a star particle of  $20 M_\odot$ , suggesting that the number of star particles in our simulation is similar to the actual number of stars that contribute to Ba enrichment. Therefore we expect that the AGB stars are well-sampled and that the *s*-process element production is accurately followed.

We also note that, in our model, Sr is produced only in AGB stars, although various channels for Sr production are proposed (see, e.g. [Wanajo et al. 2011](#)). In the present study, we mainly consider the Ba enrichment for which the production is dominated by AGB stars. For detailed discussion on Sr modeling in dwarf galaxies, see [Hirai et al. \(2019\)](#).

## 3 RESULTS

### 3.1 Star formation duration and abundance of [Ba/Fe] and [Sr/Fe]

Fig. 2 presents the abundance ratio of neutron-capture elements [Ba/Fe] and [Sr/Fe] as a function of [Fe/H] for stars in MW halo and in dwarf galaxies. All the simulation results are snapshots at  $z = 6.4$ . We define ‘Ba-poor’ stars as stars with upper limits on Ba abundance or stars with  $[\text{Ba}/\text{Fe}] < -1.5$ . The observed fraction of Ba-poor stars is 45 per cent. The median lines derived from our model stars clearly show the deficit of Ba and Sr abundances compared to the observations. In the large UFD, the Ba-poor fraction is 76 per cent, and in the small UFD the fraction is 100 per cent. The epoch of star formation (shown by the colours of the dots) reflects the chemical enrichment of iron and *s*-process elements. The dependence of chemical enrichment on the epoch of star formation is more

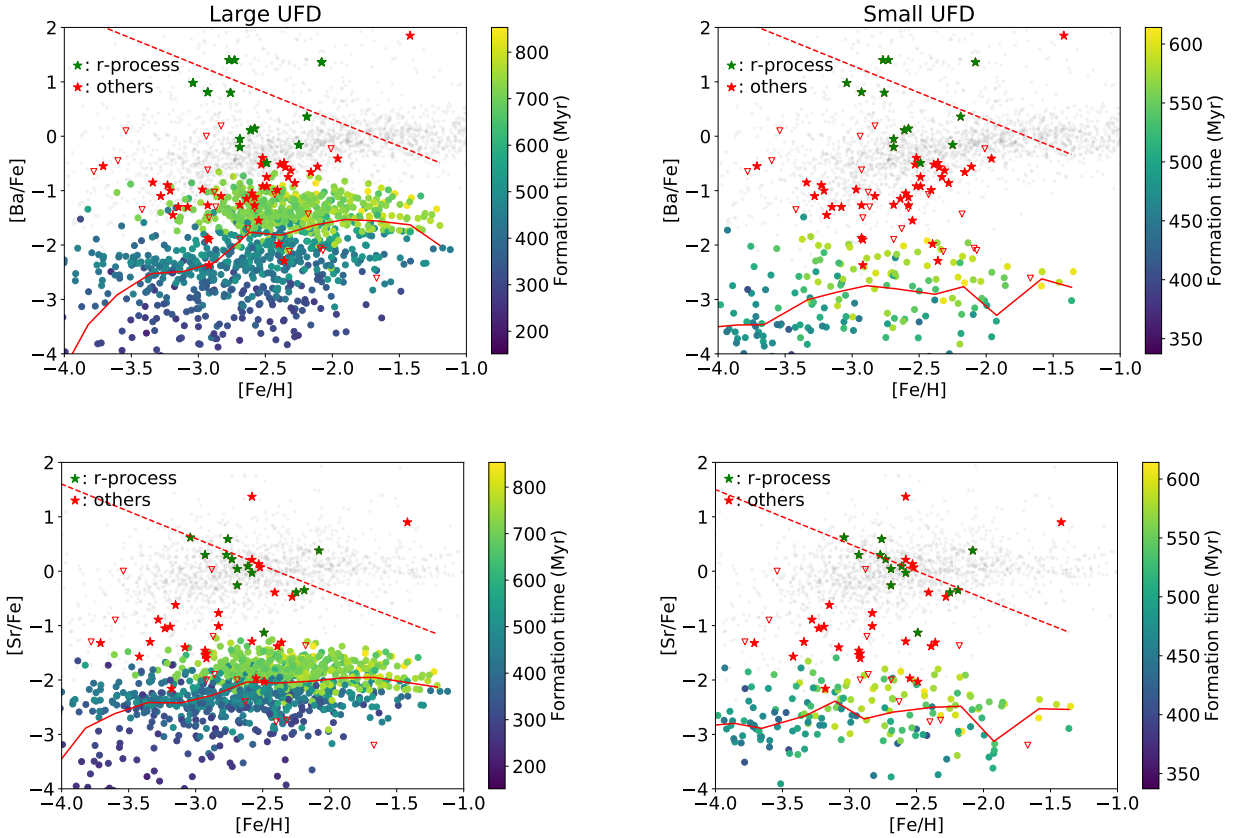


**Figure 2.**  $[\text{Ba}/\text{Fe}]$  (top panels) and  $[\text{Sr}/\text{Fe}]$  (bottom panels) as a function of  $[\text{Fe}/\text{H}]$  for model stars in our two UFD models (circles) at  $z = 6.4$ , compared with the observational data of stars in UFDs (stars and triangles). The red solid lines show the median of  $[\text{Ba}/\text{Fe}]$  and  $[\text{Sr}/\text{Fe}]$  in each  $[\text{Fe}/\text{H}]$  bin for model stars. The red dashed lines show the median of  $[\text{Ba}/\text{Fe}]$  ( $[\text{Sr}/\text{Fe}]$ ) in each  $[\text{Fe}/\text{H}]$  bin for model stars, after a "boost" assuming that an  $r$ -process event enriched the galaxy to  $[\text{Ba}/\text{H}] = -1.7$  ( $[\text{Sr}/\text{H}] = -2.5$ ). The bin size is 0.25 dex. The left and right panels show the data of 'large UFD', and 'small UFD', respectively. Observational data are obtained from the SAGA database (Suda et al. 2008, 2017), together with the latest data added manually. The data are originally obtained by the following literature: (Martin et al. 2007; Koch et al. 2008; Adén et al. 2009; Feltzing et al. 2009; Koch et al. 2009; Frebel et al. 2010; Norris et al. 2010c,a,b; Adén et al. 2011; Lai et al. 2011; Simon et al. 2011; Gilmore et al. 2013; Koch et al. 2013; Vargas et al. 2013; Frebel et al. 2014; Ishigaki et al. 2014; Koch & Rich 2014; François et al. 2016; Ji et al. 2016b,d,c; Martin et al. 2016; Roederer et al. 2016; Hansen et al. 2017; Kirby et al. 2017; Venn et al. 2017; Chiti et al. 2018; Ji & Frebel 2018; Nagasawa et al. 2018; Ji et al. 2019b; Hansen et al. 2020). The stars that show the characteristic abundance patterns for the  $r$ -process (seven stars from Ret II, five stars from Tuc III, and one star from Grus II) are plotted with green star symbols, and other stars are plotted with red star symbols. The list of UFDs are: Bootes I, Bootes II, Canes Venatici II, Coma Berenices, Grus I, Hercules, Horologium I, LeoIV, Pisces II, Reticulum II, Segue 1, Segue 2, Triangulum II, Tucana II, Tucana III, Ursa Major, Ursa Major II, and Willman I. Stars with only upper limits available are plotted with open triangles.

pronounced in  $[\text{Ba}/\text{Fe}]$  than in  $[\text{Sr}/\text{Fe}]$ . This is likely a consequence of the enhanced production of Sr in massive end of AGB stars.

UFDs can be classified by whether the  $r$ -process has a dominant effect on their chemical evolution. Reticulum II (Ret II), Tucana III (Tuc III) and Grus II (Gru II) are the ones with clear signatures of the  $r$ -process.<sup>1</sup> Stars in these UFDs (plotted in green) show higher Ba and Sr abundances than those in other UFDs (plotted in red). Since Ba and Sr are also produced in the  $r$ -process, it is natural that their abundances are systematically higher. We plot a dashed line showing the change of the median values along  $[\text{Fe}/\text{H}]$  for UFDs that experience a single  $r$ -process event in the past. The large amounts of Ba and Sr produced by the  $r$ -process event wash out any information on previous neutron-capture processes in stars that form afterwards.

<sup>1</sup> There is one star with a significant Eu and Ba enhancement in Segue 1. It is a CH star, and the high abundance of the neutron-capture elements is thought to originate from mass transfer from the former AGB star in a binary system and not by previous neutron-capture processes.

The abundance of  $s$ -process elements show large variation even among our simulated UFDs, which are uncontaminated by  $r$ -process enrichment. Ba and Sr abundances are higher in the large UFD than in the small UFD, even if we compare the stars with similar Fe abundances. The different abundances reflect the difference in the star formation histories. The large UFD forms stars for 600 Myr, whereas the small UFD quenches after 300 Myr of star formation. In galaxies with long star formation duration, elements that low-mass stars synthesize are taken into the stars that form later. Therefore the abundances of  $s$ -process elements are higher in the large UFD due to the larger contribution from low-mass stars.

### 3.2 Scatter of $[\text{Ba}/\text{Fe}]$ and $[\text{Sr}/\text{Fe}]$

Typically the scatter of  $[\text{Ba}/\text{Fe}]$  among stars within a galaxy is less than 1 dex for observed UFDs. The observed scatter is typically small compared to our simulated galaxy samples, whose Ba enrichment occurs only through AGB stars. In terms of the scatter, the small

UFD, in which a single star-formation "burst" is quenched after a duration of 300Myr, is more similar to the observations than the large UFD. We can see an increase of [Ba/Fe] as the evolutionary time increases in the simulated galaxies. The abundance plots for the large UFD (see left panels in Fig. 2) show two distinct populations which correspond to two star bursts that the galaxy experiences (see Fig. 1). [Ba/Fe] and [Sr/Fe] differ by roughly 1.5 and 1 dex between these populations. Considering that even within each population there is a scatter of  $\sim 0.5$  dex, this additional factor would make the scatter too large. There are two ways to reconcile: one is to assume that stars in the observed UFDs are mostly formed in a single short ( $\sim 100$  Myr) burst, and the other is to enhance the Ba and Sr abundance of the first stellar population. We will discuss this further in the next section.

As shown by the points with similar formation times in Fig. 2, our models predict the distribution in a wide range of [Fe/H], while the variation in [Ba/Fe] is not large compared to [Fe/H] scatter among stars with similar ages. This suggests that (i) the elements are sufficiently well-mixed in metal-rich regions, but (ii) the mixing of metal-rich and metal-poor portions occurs slowly. There is an interesting difference between the *s*- and *r*-processes in terms of chemical signature in UFD. Since the *r*-process occurs at most once or a few times in these small systems, the spatial position is important (Tarumi et al. 2020). The scatter of [Eu/Fe] in each UFD is a consequence of inhomogeneous mixing among different elements. In contrast, *s*-process elements originate in low-mass stars, which are formed quite often. Therefore they enrich a galaxy relatively homogeneously. The [Ba/Fe] scatter among stars within each UFD rather reflects different formation epochs of the stars. Note that the IMF-averaging in our simulations could artificially make Ba distribution homogeneous. A further investigation is required to obtain a solid conclusion on the spatial inhomogeneity of *s*-process elements.

We find smaller [Sr/Fe] scatters in our simulations. This is consistent with stellar models where Sr is also synthesized in an environment with a relatively smaller neutron exposure, which allows massive AGB stars to synthesize them. Production and dispersal of Sr begin earlier than those of Ba, and thus even stars formed very early are enriched with Sr. It makes the difference of [Sr/Fe] between the early and late stellar populations smaller.

## 4 DISCUSSION

### 4.1 *r*-process contribution

The *s*-process enrichment of MW stars has been studied for decades (e.g. Cescutti et al. 2006). In our model, a major portion of *s*-process elements are produced in the AGB phase of low-mass stars with  $M \lesssim 3 M_{\odot}$ . Because of the long delay-time and the strong metallicity dependence of the Ba yield from the AGB stars, other production paths such as the *r*-process are preferred as the origin of Ba in low metallicity stars. Previous simulations (e.g. Cescutti et al. 2006) suggest that, for MW stars with  $-3 < [\text{Fe}/\text{H}] < -2$ , Ba is predominantly produced by the *r*-process. A similar conclusion is obtained by Hirai et al. (2019), who study the production of Sr in classical dwarf galaxies.

The story is different for UFDs. Due to their small stellar masses, the rarity of the *r*-process considerably alters the stellar abundances: the number of *r*-process events in a UFD is likely one at most. This stochasticity of *r*-process in each UFD is needed to explain the extremely high Eu abundance of Ret II, and an apparent "jump" in the Eu abundance observed in Gru II. The moderate Eu abundance

of Tuc III could also be explained by assuming that the *r*-process event occurred in the outskirts (Tarumi et al. 2020), or that the *r*-process elements are diluted to a larger mass of hydrogen than in Ret II (Marshall et al. 2018). Interestingly, the large scatter of Eu abundance among low-metallicity halo stars can also be explained by rare *r*-process enrichment. The dashed lines in Fig. 2 suggest that stars with a clear signature of *r*-process enrichment should also have high Ba abundances. This is consistent with the results obtained from the chemical evolution modeling of the MW, i.e. at the metallicities of UFDs the *r*-process is the dominant source of Ba. Following this picture, we can exclude the contribution from the 'rare and prolific *r*-process events' for stars of UFDs with low Eu abundances.

### 4.2 Ba production in UFDs

We compare the stellar Ba abundances of the observed and simulated UFDs. We find the median is [Ba/Fe]  $\sim -2$  (large UFD) and [Ba/Fe]  $\sim -3$  (small UFD) for stars with  $-3 < [\text{Fe}/\text{H}] < -2$  (see Fig. 2). The [Ba/Fe] are the same as the yield from a single stellar populations (SSP) integrated from the birth to the age of 100 Myr (large UFD) and 50 Myr (small UFD). We obtain similar conclusions if we use [Sr/Fe] instead. Note that the estimated age is insensitive to the exact choice of the yields, as it does not affect star formation in the galaxy. Even if we change the Ba yields from AGB stars, we expected that the typical [Ba/Fe] of stars formed in these galaxies are represented by [Ba/Fe] of an SSP at 100 (50) Myr. Also, [Ba/Fe] is homogeneous within metal-rich regions at any moment. Therefore we conclude that the SSP age and star formation history of the system are two important factors that affect [Ba/Fe] in the UFDs.

The duration of star formation in UFDs can be naively constrained to up to a few hundred Myr because gas heating by cosmic reionization can effectively quench star formation in these small galaxies by  $z \sim 6$ . In addition, considering their low halo masses, we do not expect the onset of star formation in UFDs to be extremely early. Typically in our simulations, star formation begins when the cosmic age is about 300 Myr. With these conditions the duration of star formation in UFDs is shorter than 700 Myr. In our simulations, the 'large UFD' has comparable length of star formation. Therefore the large UFD can be considered as one of the most *s*-process enhanced UFDs. However, the predicted Ba abundance is still smaller than the observed values. This suggests that Ba needs to be produced more efficiently in low-metallicity environments such as UFDs.

A simple resolution to enhance Ba production might be to adopt different AGB yields. It may solve the inconsistency in the absolute amounts of Ba accumulated in the entire galaxies, but unfortunately, it does not mitigate the discrepancy in terms of the scatter of [Ba/Fe] in each galaxy. In order to reproduce the small scatter found in the observations, the galaxies need to have short durations of star formation. According to our model, UFDs experiencing star formation for more than  $\sim 200$  Myr are expected to show a scatter in [Ba/Fe] of more than 1 dex. If Ba is produced only by low-mass AGB stars, the duration of star formation in UFDs should be shorter than 200 Myr, and then Ba production should be more efficient by a factor of 10-100.

Another candidate of Ba source is super-AGB stars (Doherty et al. 2017). The typical mass of the progenitors is 6-8  $M_{\odot}$ , and thus super-AGB stars produce *s*-process elements within 100 Myr of their evolution. We employ the *s*-process yields from Doherty et al. (2017) (C. Doherty, priv. comm.) and re-calculate the stellar elemental abundances. We have found only a minor contribution of super-AGB stars to the production of Ba and Sr, as shown in Fig. A1. This is owing to the narrow mass range of the progenitors and less-efficient *s*-process

element production in super-AGB stars. Although super-AGB stars enable early *s*-process enrichment, the absolute amounts of Ba in UFDs do not increase significantly. In order for super-AGB stars to be the main source of Ba in UFDs, the yield should be enhanced by a large factor of  $\sim 10$ .

The IMF of stars in metal-poor environments such as UFDs could be different from the present-day IMF (Gennaro et al. 2018). Komiya et al. (2009) propose a log-normal IMF centered at  $3\text{--}20 M_{\odot}$ , to explain the fraction of *s*-process enhanced stars in carbon-enhanced metal-poor stars in the MW. As a simple test, we adopt this form of IMF and examine how the abundances of the *s*-process elements are affected. Fig. 3 shows the Ba abundances in the model with a modified IMF similar to Komiya et al. (2007). The IMF is log-normal centred at  $4 M_{\odot}$  with a standard deviation of 0.1 dex. We note that, in addition to the stars of this IMF, low-mass companions in binary systems are assumed to be formed and to survive until today, but the companions are not explicitly represented in our simulations. The production of Fe is suppressed, and that of Ba from super-AGB stars is enhanced, which results in the enhancement of  $[\text{Ba}/\text{Fe}]$ . Also, the delay time of the Ba production and dispersal in the interstellar medium is shorter than in the case with a typical IMF due to the birth of many super-AGB stars that produce *s*-process elements on short timescales.

An interesting connection of this peculiar IMF is the multiple populations in globular clusters (GCs). Their peculiar chemical abundances can be explained by the contribution from super-AGB stars to the chemical enrichment before the formation of second generation stars (see, e.g. Bastian & Lardo 2018). There are also implications for other issues such as the mass-budget problem, in which the ratios of the total mass of first-generation stars to second-generation stars is anomalous (Renzini 2008). The log-normal IMF, which has a large mass fraction of super-AGB stars, could alleviate the mass-budget problem. Also, the IMF greatly reduces the production of iron. Therefore the metallicities do not significantly differ between the first generation stars and the second generation stars. We still cannot conclude that the IMF presented by Komiya et al. (2007) is a viable solution because the application of the different IMF is supported for stars with  $[\text{Fe}/\text{H}] < -2$  (Suda et al. 2013; Lee et al. 2014), which is inconsistent with the fact that the majority of stars in GCs have  $[\text{Fe}/\text{H}] > -2$ . However, it is interesting that enhancing the fraction of super-AGB stars while decreasing massive stars is favoured in a completely different context of UFD chemical evolution.

Yet another possibility is to incorporate the contribution of massive stars that produce Ba on short timescales. The need for Ba production by objects with short lifetimes is also pointed out by Ji et al. (2019a) who show that all the known UFDs for which it has been attempted to measure Ba abundances are enriched to  $[\text{Ba}/\text{H}] \gtrsim -5$ . Rotating massive star (RMS) models have been invoked for efficient production of *s*-process elements in recent studies (see, e.g. Choplin et al. 2018). Massive stars that die as supernovae can promptly pollute the interstellar medium in the early epoch of galaxy evolution. Such prompt enrichment can enhance the overall Ba abundance, but also prevents from producing large scatter of  $[\text{Ba}/\text{Fe}]$  among stars in a galaxy. In Fig. 4 we show the result for an *ad hoc* model in which  $3 \times 10^{-10} M_{\odot}$  of Ba per  $1 M_{\odot}$  of formed stellar mass is produced from massive ( $> 8 M_{\odot}$ , short-lived) stars. The median line roughly matches the distribution of observed UFD abundances. The scatter among different UFDs may provide insight into the *s*-process enrichment, which we further discuss in the next subsection.

The high Ba abundances in UFDs may be the evidence of multiple *r*-process origins. Recent observations reveal that  $[\text{Ba}/\text{Fe}]$  does not increase as  $[\text{Fe}/\text{H}]$  increases for stars in MW with  $-2.0 < [\text{Fe}/\text{H}]$

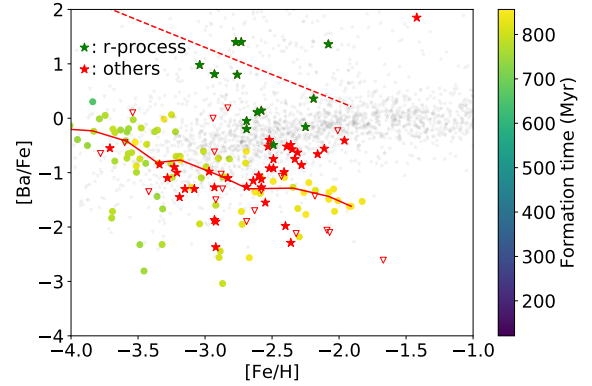


**Figure 3.** Model with modified IMF (log-normal, centered at  $4.0 M_{\odot}$ , with a standard deviation of 0.1 in log-space). Due to a larger fraction of stars that experience a super-AGB phase and a smaller fraction of stars that explode,  $[\text{Ba}/\text{Fe}]$  is higher than in the case of a typical IMF. Observational data are shown with the same symbols as in Fig. 2.

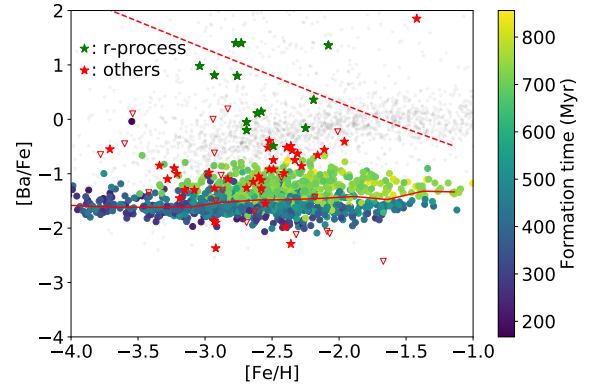


**Figure 4.** Model with an additional Ba source originating from massive stars. We assume that the amount of Ba produced per  $1 M_{\odot}$  of stars is  $3 \times 10^{-10} M_{\odot}$ . The additional Ba contribution reproduces the typical values of  $[\text{Ba}/\text{Fe}]$  in UFDs. On the other hand, it is suggested that the source of Ba in some UFDs with low  $[\text{Ba}/\text{Fe}]$  is relatively rare stars, and that the stellar masses of UFDs (e.g. Segue 1) are not enough to well-sample such stars.

$< -1.5$ , suggesting that *s*-process yields from AGB stars do not contribute to stars with  $[\text{Fe}/\text{H}] < -1.5$  (Matsuno et al. 2020). However, the  $[\text{Eu}/\text{Ba}]$  of their sample stars is lower than the value predicted by *r*-process nucleosynthesis. This may suggest that there are some *s*-process events which produce Ba with a delay-time similar to the timescale of the metal enrichment leading to  $[\text{Fe}/\text{H}] \sim -1.5$ . An interesting test of this possibility would be to measure or place constraints on Eu abundances for stars with measured Ba abundances in UFDs, so that we can identify the main contributors of Ba as originating from the *r*- or *s*-processes.

### 4.3 Diversity of UFDs

The large difference in the Ba abundances among UFDs provides an interesting clue. The values of  $[\text{Ba}/\text{Fe}]$  in UFDs range from  $-0.5$  (e.g. Bootes I) to  $-2$  (e.g. Segue 1) with a scatter of 1.5 dex. This is

larger than those of other elements such as magnesium or calcium which are commonly synthesized in massive stars. Our models do *not* well reproduce the variations of [Ba/Fe] in UFDs. If we assume that (i) the stellar yields, (ii) the (initial) mass function of the stars, and (iii) the star formation history are the same or similar among all the UFDs, the resulting [Ba/Fe] cannot be significantly different. We may also presume that the stellar yields are the same among UFDs with similar stellar masses and metallicities. The IMF can make a difference, directly or through the delay-time of the Ba enrichment. However, as is shown in Fig. 3, reproducing the Ba abundances of UFDs by varying the IMF alone requires fine tuning. Also, we are not strongly motivated to consider IMF variation in UFDs because Fe abundances in UFDs are similar to each other. The diversity of the star formation histories can make a difference if the Ba enrichment occurs with a significant delay-time. AGB stars seem to be the natural sources, but we have shown that the Ba abundances in UFDs cannot be explained by the contribution of AGB stars alone.

Another source of diversity is stochasticity. If stellar masses present in UFDs are not enough to well-sample the IMF, the ‘Poisson error’ can lead to an apparent diversity in the perceived IMFs. For example, the luminosity of Segue 1, which is a UFD of the lowest [Ba/Fe], is  $\sim 300L_{\odot}$ . Fast-rotating massive stars could be such rare and prolific Ba contributors. According to Choplin et al. (2018), a  $25 M_{\odot}$  star rotating at 70 per cent of the critical rotation speed with the mass\_cut of  $5 M_{\odot}$  produces  $3 \times 10^{-7} M_{\odot}$  of Ba. If we assume that such a star is born every  $1000 M_{\odot}$  of stars formed, we can explain the Ba abundances of most UFDs while allowing low-Ba systems to also exist due to stochastic enrichment. Although the evolutionary models of rotating stars include parameters that are poorly constrained, identifying the origin of Ba in UFDs may also provide invaluable information on the properties of massive rotating stars.

#### 4.4 Effects of tidal stripping

Signatures of tidal stripping are observed in some UFDs. If tidal stripping is common among UFDs, their stellar masses could be significantly higher than we assume ( $\sim 10^5 M_{\odot}$ ) before the stripping. In this case they could be so massive that the stochasticity of  $r$ -process is averaged out. Also their potential well could be significantly deeper, allowing them to keep forming stars after the cosmic reionization. Therefore our working hypotheses regarding short star formation timescales and ‘0 or 1’  $r$ -process break down. Bootes I and Ursa Major II, which have stars with [Ba/Fe]  $> -1$ , may have lost their stellar mass by tidal force by the MW (Belokurov et al. 2006; Zucker et al. 2006). It is possible that such UFDs were initially more massive, therefore were able to form stars even after the reionization, accumulating  $s$ -process elements. Also such systems can have enough mass to average out the stochasticity of  $r$ -process. The failure of our model to reproduce [Ba/Fe]  $\sim -0.5$  stars might imply that Ba-rich UFDs are actually such tidally disrupted systems. However, most UFDs are too far away from the Galactic centre to lose their stars (Simon 2018). Also, there are UFDs with [Ba/Fe]  $\sim -1$  that do not show signatures of a disruption event. In this paper we assume that most of the UFDs have retained most of the stars formed within them.

#### 4.5 Sr production in UFDs

Sr is lighter than Ba and thus can be synthesized in less extreme conditions (e.g. ‘light-element primary process’, Montes et al. 2007). Such ‘exclusive’ sources of Sr may be necessary to explain the existence

of stars with Sr enhancement compared to heavier elements such as Ba or Eu (Honda et al. 2004). Hirai et al. (2019) consider electron-capture SNe and RMS as additional sources of Sr. They conclude that the additional Sr production in short-lived stars is necessary to explain the Sr abundances in dwarf galaxies.

In our simulations, Sr is only produced in AGB stars. Fig. 2 shows the same trend for Ba. A sufficient amount of Sr is not produced in our models. Although we cannot identify the origin(s) of Sr, we can estimate the required Sr mass. To explain the observed Sr abundances ([Sr/Fe]  $\sim -1$ ), the Sr yield required is  $10^{-8} M_{\odot}$  per  $1 M_{\odot}$  of stars in the first 100 Myr. Considering the large difference of Sr abundances among the UFDs, we argue that there may exist a production source of Sr that is rare and prolific.

## 5 CONCLUSIONS

We focus on the production of Ba in UFDs. First, our basic assumption is that most of the UFDs do not experience any  $r$ -process events so that all the Ba content originates from the  $s$ -process in AGB stars. Even though we use one of the most up-to-date set of elemental yields that explain  $s$ -process enrichment in the MW, Ba and Sr abundances in UFDs are not reproduced. Our findings are summarized as follows.

(i) Ba should be produced efficiently ( $\sim 3 \times 10^{-10} M_{\odot}$  per  $1 M_{\odot}$  of stars in the first 100 Myr) even in low-metallicity environments such as UFDs. The required short delay-time suggests that the origin of Ba has a short evolutionary timescale such as massive stars. Super-AGB stars alone cannot resolve the inconsistency between our simulation result and observations.

(ii) The observed scatter of [Ba/Fe] ( $\sim 1$  dex) is small considering the typical star formation histories of the host UFD. This problem is mitigated if we assume another source of Ba which contributes with little or no delay time.

(iii) By introducing an IMF which makes predominantly super-AGB and AGB stars while suppressing the Fe production by massive stars, we can explain the Ba abundances. However, fine tuning is needed to determine the IMF, and a rather peculiar one is preferred.

Future observations of additional stars in UFDs will allow us to identify the origin of Ba and  $s$ -process elements. UFDs serve as an important laboratory for nucleosynthesis in the early Universe.

## ACKNOWLEDGEMENTS

We thank Volker Springel for kindly providing the simulation code AREPO, Jill Naiman for assembling yield table for  $s$ -process elements, and Carolyn Doherty for kindly sharing her yield table of super-AGB stars. We thank Shinya Wanajo, Yutaka Hirai, Kenta Hotokezaka, Yutaka Komiyama, Masayuki Fujimoto, and Anna Frebel for fruitful discussions. This study was supported by World Premier International Research Center Initiative (WPI), MEXT, Japan and by SPPEXA through JST CREST JPMHCR1414. The numerical computations presented in this paper were carried out on Cray XC50 at Center for Computational Astrophysics, National Astronomical Observatory of Japan. TS was supported by JSPS KAKENHI Grant Numbers 20HP8012 and 16H02166. FvdV acknowledges support from the Deutsche Forschungsgemeinschaft through project SP 709/5-1 and from a Royal Society University Research Fellowship.

## DATA AVAILABILITY

The data underlying this article will be shared on reasonable request to the corresponding author.

## REFERENCES

- Adén D., et al., 2009, *A&A*, **506**, 1147  
 Adén D., Eriksson K., Feltzing S., Grebel E. K., Koch A., Wilkinson M. I., 2011, *A&A*, **525**, A153  
 Bastian N., Lardo C., 2018, *ARA&A*, **56**, 83  
 Belokurov V., et al., 2006, *ApJ*, **647**, L111  
 Brown T. M., et al., 2014, *ApJ*, **796**, 91  
 Cescutti G., François P., Matteucci F., Cayrel R., Spite M., 2006, *A&A*, **448**, 557  
 Chabrier G., 2001, *ApJ*, **554**, 1274  
 Chiti A., Frebel A., Ji A. P., Jerjen H., Kim D., Norris J. E., 2018, *ApJ*, **857**, 74  
 Choplin A., Hirschi R., Meynet G., Ekström S., Chiappini C., Laird A., 2018, *A&A*, **618**, A133  
 Cowan J. J., Sneden C., Lawler J. E., Aprahamian A., Wiescher M., Langanke K., Martínez-Pinedo G., Thielemann F.-K., 2019, arXiv e-prints, p. arXiv:1901.01410  
 Cristallo S., Straniero O., Piersanti L., Gobrecht D., 2015, *ApJS*, **219**, 40  
 Cristallo S., Karinkuzhi D., Goswami A., Piersanti L., Gobrecht D., 2016, *ApJ*, **833**, 181  
 Doherty C. L., Gil-Pons P., Siess L., Lattanzio J. C., 2017, *Publ. Astron. Soc. Australia*, **34**, e056  
 Feltzing S., Eriksson K., Kleya J., Wilkinson M. I., 2009, *A&A*, **508**, L1  
 François P., Monaco L., Bonifacio P., Moni Bidin C., Geisler D., Sbordone L., 2016, *A&A*, **588**, A7  
 Frebel A., Simon J. D., Geha M., Willman B., 2010, *ApJ*, **708**, 560  
 Frebel A., Simon J. D., Kirby E. N., 2014, *ApJ*, **786**, 74  
 Gennaro M., et al., 2018, *ApJ*, **855**, 20  
 Gilmore G., Norris J. E., Monaco L., Yong D., Wyse R. F. G., Geisler D., 2013, *ApJ*, **763**, 61  
 Grand R. J. J., et al., 2017, *MNRAS*, **467**, 179  
 Hahn O., Abel T., 2011, *MNRAS*, **415**, 2101  
 Hansen T. T., et al., 2017, *ApJ*, **838**, 44  
 Hansen T. T., et al., 2020, arXiv e-prints, p. arXiv:2005.10767  
 Hirai Y., Wanajo S., Saitoh T. R., 2019, *ApJ*, **885**, 33  
 Honda S., Aoki W., Kajino T., Ando H., Beers T. C., Izumiura H., Sadakane K., Takada-Hidai M., 2004, *ApJ*, **607**, 474  
 Ishigaki M. N., Aoki W., Arimoto N., Okamoto S., 2014, *A&A*, **562**, A146  
 Ji A. P., Frebel A., 2018, *ApJ*, **856**, 138  
 Ji A. P., Frebel A., Chiti A., Simon J. D., 2016a, *Nature*, **531**, 610  
 Ji A. P., Frebel A., Simon J. D., Geha M., 2016b, *ApJ*, **817**, 41  
 Ji A. P., Frebel A., Simon J. D., Chiti A., 2016c, *ApJ*, **830**, 93  
 Ji A. P., Frebel A., Ezzeddine R., Casey A. R., 2016d, *ApJ*, **832**, L3  
 Ji A. P., Simon J. D., Frebel A., Venn K. A., Hansen T. T., 2019a, *ApJ*, **870**, 83  
 Ji A. P., Simon J. D., Frebel A., Venn K. A., Hansen T. T., 2019b, *ApJ*, **870**, 83  
 Karakas A. I., Lugaro M., 2016, *ApJ*, **825**, 26  
 Kirby E. N., Cohen J. G., Simon J. D., Guhathakurta P., Thygesen A. O., Duggan G. E., 2017, *ApJ*, **838**, 83  
 Koch A., Rich R. M., 2014, *ApJ*, **794**, 89  
 Koch A., McWilliam A., Grebel E. K., Zucker D. B., Belokurov V., 2008, *ApJ*, **688**, L13  
 Koch A., et al., 2009, *ApJ*, **690**, 453  
 Koch A., Feltzing S., Adén D., Matteucci F., 2013, *A&A*, **554**, A5  
 Komiya Y., Suda T., Minaguchi H., Shigeyama T., Aoki W., Fujimoto M. Y., 2007, *ApJ*, **658**, 367  
 Komiya Y., Suda T., Fujimoto M. Y., 2009, *ApJ*, **694**, 1577  
 Lai D. K., Lee Y. S., Bolte M., Lucatello S., Beers T. C., Johnson J. A., Sivarani T., Rockosi C. M., 2011, *ApJ*, **738**, 51  
 Lee Y. S., Suda T., Beers T. C., Stancliffe R. J., 2014, *ApJ*, **788**, 131

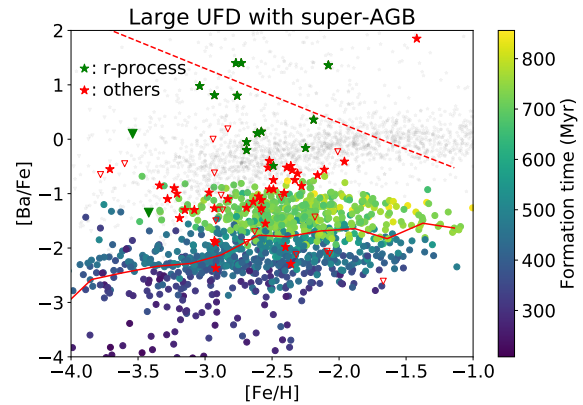


**Figure A1.** Model with Ba production from super-AGB stars. It enhances [Ba/Fe] slightly, but not sufficiently to explain the observed UFD abundances.

- Marshall J., et al., 2018, arXiv e-prints, p. arXiv:1812.01022  
 Martin N. F., Ibata R. A., Chapman S. C., Irwin M., Lewis G. F., 2007, *MNRAS*, **380**, 281  
 Martin N. F., et al., 2016, *ApJ*, **818**, 40  
 Matsuno T., et al., 2020, arXiv e-prints, p. arXiv:2006.03619  
 Montes F., et al., 2007, *ApJ*, **671**, 1685  
 Nagasawa D. Q., et al., 2018, *ApJ*, **852**, 99  
 Nishimura N., Sawai H., Takiwaki T., Yamada S., Thielemann F. K., 2017, *ApJ*, **836**, L21  
 Norris J. E., Yong D., Gilmore G., Wyse R. F. G., 2010a, *ApJ*, **711**, 350  
 Norris J. E., Gilmore G., Wyse R. F. G., Yong D., Frebel A., 2010b, *ApJ*, **722**, L104  
 Norris J. E., Wyse R. F. G., Gilmore G., Yong D., Frebel A., Wilkinson M. I., Belokurov V., Zucker D. B., 2010c, *ApJ*, **723**, 1632  
 Pakmor R., Springel V., Bauer A., Mocz P., Munoz D. J., Ohlmann S. T., Schaal K., Zhu C., 2016, *MNRAS*, **455**, 1134  
 Planck Collaboration et al., 2018, arXiv e-prints, p. arXiv:1807.06209  
 Renzini A., 2008, *MNRAS*, **391**, 354  
 Roederer I. U., et al., 2016, *AJ*, **151**, 82  
 Safarzadeh M., Ji A. P., Dooley G. A., Frebel A., Scannapieco E., Gómez F. A., O’Shea B. W., 2018, *MNRAS*, **476**, 5006  
 Simon J. D., 2018, *ApJ*, **863**, 89  
 Simon J. D., 2019, arXiv e-prints, p. arXiv:1901.05465  
 Simon J. D., et al., 2011, *ApJ*, **733**, 46  
 Springel V., 2010, *MNRAS*, **401**, 791  
 Suda T., et al., 2008, *PASJ*, **60**, 1159  
 Suda T., et al., 2013, *MNRAS*, **432**, L46  
 Suda T., et al., 2017, *PASJ*, **69**, 76  
 Tarumi Y., Yoshida N., Inoue S., 2020, *MNRAS*, **494**, 120  
 Vargas L. C., Geha M., Kirby E. N., Simon J. D., 2013, *ApJ*, **767**, 134  
 Venn K. A., Starkeburg E., Malo L., Martin N., Laevens B. P. M., 2017, *MNRAS*, **466**, 3741  
 Wanajo S., Janka H.-T., Müller B., 2011, *ApJ*, **726**, L15  
 Weinberger R., Springel V., Pakmor R., 2019, arXiv e-prints, p. arXiv:1909.04667  
 Zucker D. B., et al., 2006, *ApJ*, **650**, L41

## APPENDIX A: SUPER-AGB

In Fig. A1 we show the result of model that take Ba production from super-AGB stars into account. The symbols are the same as in Fig. 2. It enhances [Ba/Fe] at [Fe/H] < -3, but not significantly at [Fe/H]  $\gtrsim$  -3.

This paper has been typeset from a  $\text{\TeX/L\AA\TeX}$  file prepared by the author.